Investigating Mechanical Behaviors of Silica Nanoparticle Reinforced Composites

Jia-Lin Tsai, Hung Hsiao and Yi-Lieh Cheng

Journal of Composite Materials 2010 44: 505 originally published online 3 September 2009
DOI: 10.1177/0021998309346138

Investigating Mechanical Behaviors of Silica Nanoparticle Reinforced Composites

JIA-LIN TSAI,* HUNG HSIAO AND YI-LIEH CHENG
Department of Mechanical Engineering
National Chiao Tung University, Hsinchu 300, Taiwan

ABSTRACT: The research is aimed to investigate the mechanical behaviors of epoxy-based nanocomposites reinforced with spherical nanoparticles. Five different contents of silica nanoparticles – 5, 10, 15, 20, and 40 wt% – were introduced in the samples. Through a sol–gel technique, the silica particles with a diameter of 25 nm were exfoliated uniformly in the epoxy matrix. Experimental results obtained from tensile tests indicate that the modulus of nanocomposites increases with the increment of particulate inclusions, and the enhancing behavior is coincided with the model predictions obtained from the Mori–Tanaka micromechanical model. In addition, the fracture tests conducted on single-edge-notch bending specimens reveal that the inclusion of nanoparticles can effectively increase the fracture toughness of the nanocomposites. Furthermore, the extent of the enhancement is more appreciable in the brittle matrix system rather than in the ductile matrix system. Subsequently, by inserting the silica epoxy mixture into the unidirectional glass fiber through a vacuum hand lay-up process, the glass fiber/silica/epoxy composite samples were fabricated. Results depicted that the in-plane shear strength increases until the increment of particle loadings are up to 10 wt%. In addition, results obtained from the compression tests revealed that the glass/epoxy specimens with 20 wt% silica loading exhibit superior compressive strengths than those that do not contain any silica particles.

KEY WORDS: silica nanocomposites, fracture toughness, compressive strength, in-plane shear strength.

INTRODUCTION

WITH EXTENSIVE APPLICATIONS of polymer and its composites, the demand for materials that possess the characteristics of high stiffness and strength is increasing. In order to improve mechanical properties, spherical particles have been used as reinforcement in polymeric materials for many years. In general, these composite materials were reinforced with micron-sized inclusions. However, with the advance of nanotechnology

*Author to whom correspondence should be addressed. E-mail: jialin@mail.nctu.edu.tw
Figures 5, 6, 14 and 16–19 appear in color online: http://jcm.sagepub.com

0021-9983/10/04 0505–20 $10.00/0 DOI: 10.1177/0021998309346138

as well as the processing techniques, various types of particles with nanoscale have recently been developed and then utilized in conventional polymeric materials to form the nanocomposites.

In order to disperse the nanoparticles into the polymer systems with efficiency, several techniques such as mechanical shearing [1,2], mechanical mixing [3] sonication [4], and *in situ* polymerization processes [5] have been developed. Among these fabrication techniques, the silica/epoxy compound prepared through sol–gel process demonstrated a homogeneous dispersion of silica nanoparticles suspending in the epoxy resin [6]. Rosso et al. [7] employed the well-dispersed silica nanocomposites for tensile and fracture tests, indicating that the addition of 5 vol% silica nanoparticles could improve the stiffness and facture energy to 20% and 140%, respectively. The escalation behaviors were also observed by Johnsen et al. [8]. However, in their investigations, the fracture energy increased from 100 J/m^2 for the pure epoxy matrix to 350 J/m^2 for the epoxy nanocomposites with 5 vol% silica nanoparticles. Deng et al. [9] investigated the fracture behaviors of epoxy nanocomposites with nano-silica at temperature ranges from -50°C to 70°C, indicating that the fracture toughness was greatly improved at room temperature and 50°C. However, in other temperature ranges, less improvement or even declining behaviors were observed. According to the forging observation, it seems that the improvement ratio of the fracture energy with the inclusion of silica nanoparticles is dependent on the material systems employed in the nanocomposites as well as the testing environment. Considering the superior mechanical properties of silica nanoparticles, Zheng and Ning [10] adopted the silica nanocomposites as matrix material in conjunction with the glass fiber to form hybrid glass/silica/epoxy nanocomposites. They found that the bending properties as well as the tensile properties of the fiber composites were enhanced by the addition of silica nanoparticles. The enhancement could be attributed to the promoted bonding forces between the glass fiber and matrix modified by the silica nanoparticles.

In this study, systematic investigations were carried out on the silica nanocomposites as well as the glass fiber/silica/epoxy hybrid nanocomposites. For the silica nanocomposites, two different epoxy matrixes, i.e., ductile and brittle systems, were taken into account. The extent of silica particles' influence on the two different systems was demonstrated by examining the tensile, flexural, and fracture behaviors of the nanocomposites with different silica loadings. Scanning electron microscopy (SEM) and atomic force microscopy (AFM) were utilized to characterize the associated failure mechanisms. In addition, for the hybrid silica/epoxy/fiber nanocomposites system, the in-plane shear properties and the compressive behaviors that are mainly dominated by the matrix behavior were evaluated from off-axis 10° tests and uniaxial compression tests, respectively. The effects of the silica particles on the mechanical behaviors of the fiber composites were discussed.

SAMPLE PREPARATIONS

To investigate the silica nanoparticle effect on the mechanical properties of epoxy-based nanocomposites and the glass fiber/epoxy composites, the samples with various silica particle loadings were prepared. Subsequently, based on different experimental purposes, the corresponding specimens were fabricated.

Preparation of Silica/Epoxy Nanocomposites

The epoxy resin used in this study is Nanopox@ F400 supplied from Hanse Chemie, Germany. Basically, it is a diglycidyl ether of bisphenol A (DGEBA) resin, containing 40 wt% silica nanoparticles. Through sol–gel processing, the synthesized silica particles with diameters of around 25 nm were dispersed uniformly in DGEBA resin [6]. Two different curing agents were introduced in this study in an attempt to provide ductile and brittle epoxy matrixes in the nanocomposites. One is Jeffamine D-230 (polyoxypropylenedi amine with a molecular weight of 230) provided by the Huntsman Corporation, and the other is H-100 (modified cycloaliphatic amine) provided by the Yun Teh Corporation of Taiwan. When the silica/epoxy nanocomposite samples with different particle contents were prepared, the Nanopox@ F400 resin was diluted at the beginning by adding a desired amount of DGEBA resin. The mixture was then sonicated using a sonicator with cooling system around the sample container until the particles are displaced uniformly in the epoxy resin. The epoxy–silica mixture was degassed at room temperature in a vacuum oven for 10 min and then mixed with the curing agent. The mechanical stirrer was utilized to blend the final mixture at room temperature for 10 min. Again, the degassing process was conducted on the compound using a vacuum oven at 60°C for an hour to remove the embedded bubbles generated during the mechanical mixing process. Afterward, the mixture was poured into the designed steel mold with Teflon coating on its surfaces to form the nanocomposite specimens. Subsequently, the samples were cured at 100°C for 3 h with an additional 3 h at 125°C for post-curing. In the study, the nanocomposites containing 5%, 10%, 15%, 20%, and 40% loadings (by weight) of silica particles were prepared, respectively. It is noted that when nanocomposites contain high silica nanoparticle loading, the viscosity becomes higher, possibly retarding the degassing process. In order to have high quality specimens, more degassing time is suggested during the sample preparation.

Fabrication of Glass Fiber/Silica/Epoxy Nanocomposites

Vacuum-assisted hand lay-up procedures were adopted for preparing the glass fiber/silica/epoxy nanocomposites. The final mixture of silica/epoxy together with D-230 curing agent that was prepared earlier was poured on one dry unidirectional glass fiber layer (provided by Vectorply®, E-LR0908-14 unidirectional E-glass fiber). It should be noted that because of high viscosity, the H-100 curing agent was not considered for preparing the epoxy matrix used in the fiber composites. The compound was impregnated into the dry fiber by using a hand roller until the fiber bundles were permeated completely by the resin. Then another ply of dry fiber was stacked on it. The repeating process continued until the glass fiber nanocomposites were fabricated. The fiber stack was sandwiched between two steel plates with porous Teflon fabric on the surfaces, and it was then sealed within a vacuum bag. The whole laminates were cured in a hot press with suggested temperature profile under vacuum conditions. It is noted that vacuum is essential for forming nanocomposites since it can facilitate the removal of the tiny bubbles trapped in the nanocomposites during the processing. In this study, two different composite laminates were constructed in the study. One is the thin laminate (1.45 mm thick) containing five layers of glass fiber plies. The thin laminates, including 5, 10, and 20 wt% silica nanoparticles, respectively, were employed for preparing off-axis coupon specimens in the tensile tests. The other is the thick laminate (6.15 mm thick), consisting of 22 layers of fiber glass and

20 wt% silica nanoparticles. Off-axis brick specimens with fiber orientations of 0°, 5°, 10°, 15°, and 90° utilized for compression tests were then fabricated from the thick laminates.

MATERIAL CHARACTERIZATION

In order to evaluate the quality of exfoliation of the silica in the epoxy resin, the samples were examined using transmission electron microscope (TEM), which is a widespread method for providing direct visualization on the spatial distribution of the nanoparticles as well as for characterizing the microstructures of particulate nanocomposites. Thin film samples of epoxy–silica nanocomposites with 15 and 40 wt% silica particles (about 70 nm thick) were cut from the specimens, respectively, using a Reichert-Jung Ultracut E microtome, and the associated morphology were imaged using a JEOL 200CX transmission electron microscope at an accelerating voltage of 120 kV. The results with the magnification of 50 K were shown in Figure 1(a) and (b) for two different silica contents. It is noted that the sample with 15 wt% silica shown in Figure 1(a) was cured with D-230 curing agent. On the other hand, the sample shown in Figure 1(b) with 40 wt% silica loading was cured using H-100 hardener. It was found that the particles are well dispersed and homogeneouly distributed in the nanocomposites even though the particle loading is up to 40 wt%. Therefore, based on the TEM observations, it was suggested that the present samples were regarded as the nanocomposites with fully exfoliated nanoparticles.

To characterize the responses of the epoxy matrix cured with the two different curing agents, the coupon specimens were prepared in terms of the epoxy resin and the curing agents mentioned earlier. The stress and strain curves of the two samples measured from the tensile tests are illustrated in Figure 2. Apparently, the epoxy materials cured using H-100 curing agent demonstrates more stiffened and brittle behaviors rather than those cured by D-230 curing agent. In the next section, the influences of silica nanoparticles on the mechanical behavior of the two epoxy matrix were examined by performing tensile, flexural, and fracture tests.

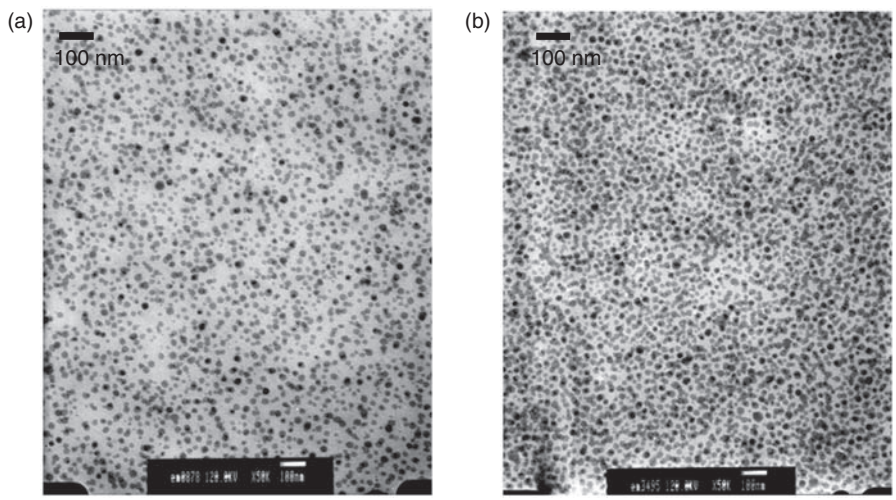

Figure 1. *TEM micrographic of the silica nanocomposites: (a) 15 wt% silica content, (b) 40 wt% silica content.*

INVESTIGATION OF MECHANICAL PROPERTIES

Silica/Epoxy Nanocomposites

TENSILE TEST

To determine the silica particle effect on the mechanical properties of epoxy resin, the tensile tests were performed on the nanocomposite coupon specimens that contain five different loadings of silica particles. Back to back strain gages were adhered on the center of the specimens to eliminate the possible bending effect as well as to measure the strain history during the tensile tests. The corresponding stress histories were obtained from the load cell mounted on the loading fixture. Figure 3 demonstrates the stress and strain curves for the epoxy and silica/epoxy systems with D-230 curing agent. It was shown that both stiffness and tensile strength increase with the increase of the silica loadings. The stress and strain curves for the brittle matrix nanocomposites (cured with H-100) with different silica loading are shown in Figure 4. It can be seen that Young's modulus increases with the increment of silica particle loading. However, the strength decreases when the silica loadings are over 20 wt%. The declining could be due to the defect generated during the fabrication process. It was found that when the silica nanoparticles were introduced into the brittle matrix because of high particle content, the compound became very sticky, making it difficult to eradiate the embedded bubbles. The influences of silica particles on the two different matrix systems measured based on tensile tests are summarized in Tables 1 and 2, respectively. No significant differences were found regarding the effect of silica nanoparticles on the tensile modulus of the two matrix systems.

The modulus of the nanocomposites with different particle contents was described using Mori–Tanaka micromechanical model [11] as:

$$C^* = (v_f C^m + v_m C^f A^{\text{Eshelby}})(v_f I + v_m A^{\text{Eshelby}})^{-1} \tag{1}$$

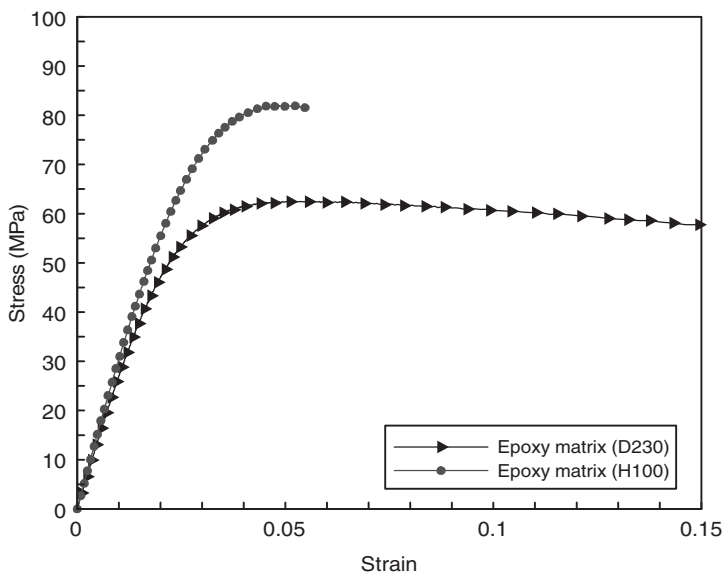

Figure 2. *Constitutive behaviors of epoxy matrix cured with D-230 and H-100 curing agent.*

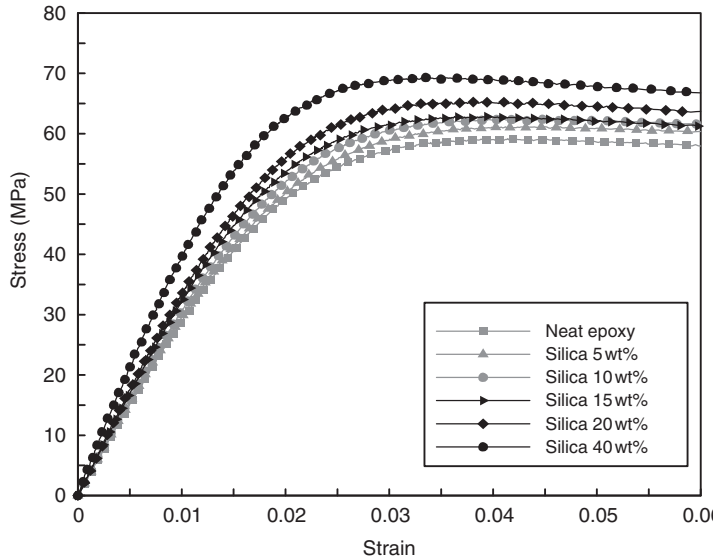

Figure 3. *Stress and strain curves for D-230 epoxy system and the corresponding nanocomposites with five different loadings of silica particles.*

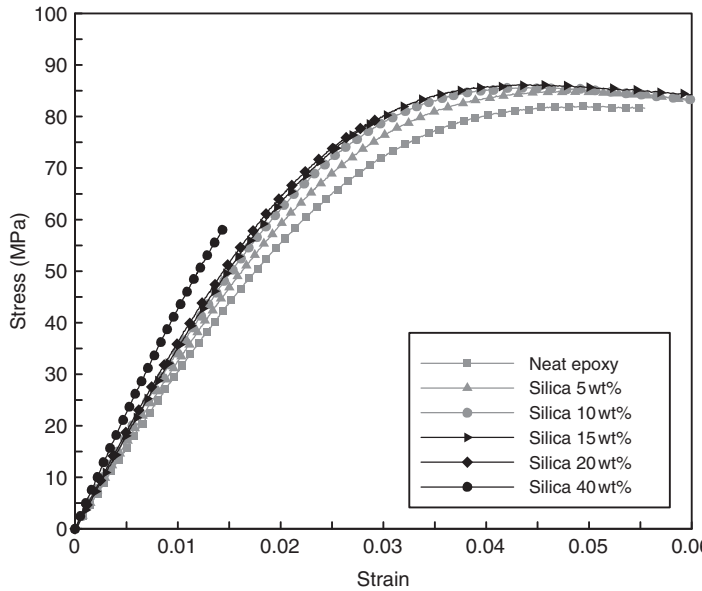

Figure 4. *Stress and strain curves for H-100 epoxy system and the corresponding nanocomposites with five different loadings of silica particles.*

where v_f and v_m are the particle and matrix volume fractions, respectively, C^f and C^m are the stiffness sensor of the particle and matrix, respectively. In addition, I is the identity tensor and A^{Eshelby} is given as:

$$A^{\text{Eshelby}} = [I + E_{\text{Esh}}(C^m)^{-1}(C^f - C^m)]^{-1} \tag{2}$$

Table 1. Effect of silica particles on Young's modulus and strength of ductile matrix nanocomposites.

Silica loading (wt%)	Young's modulus (GPa)	Increment ratio (%)	Strength (MPa)	Increment ratio (%)
0	3	–	61.3	–
5	3.2	6.7	61.6	0.5
10	3.3	10	62.5	2
15	3.4	13.3	62	1.1
20	3.5	16.7	65.3	6.5
40	4.2	40	69	12.6

Table 2. Effect of silica particles on Young's modulus and strength of brittle matrix nanocomposites.

Silica loading (wt%)	Young's modulus (GPa)	Increment ratio (%)	Strength (MPa)	Increment ratio (%)
0	3.2	–	80.7	–
5	3.4	6.3	84.2	4.3
10	3.6	12.5	81.2	0.6
15	3.7	15.6	83.7	3.7
20	3.8	18.8	76.5	–5.2
40	4.5	40.6	49.8	–38.3

where E_{Esh} is Eshelby tensor. For the spherical particles in the composites, the components of the Eshelby tensor are written explicitly as [12]:

$$E_{1111} = E_{2222} = E_{3333} = \frac{7 - 5\nu_m}{15(1 - \nu_m)} \tag{3}$$

$$E_{1122} = E_{2233} = E_{3311} = E_{1133} = E_{3322} = E_{2211} = \frac{5\nu_m - 1}{15\nu_m - 1} \tag{4}$$

$$E_{1212} = E_{2323} = E_{3131} = \frac{4 - 5\nu_m}{15(1 - \nu_m)} \tag{5}$$

where ν_m is the Poisson's ratio of the matrix.

The results obtained from the model prediction and experimental data were present in Figures 5 and 6 for ductile and brittle matrix systems, respectively. It was shown, with the dispersed nanoparticles, the modulus of the nanocomposites increases at the particles loading up to 40 wt%. Furthermore, the enhancing tendency is quite coincided with the model predictions. However, the experimental data are a little lower than the model prediction. This discrepancy could be ascribed to the local nonhomogeneity of the particle distribution within the nanocomposites, which may not be accounted for in the micro-mechanical model predictions.

THREE-POINT BENDING FLEXURE TEST

The effect of silica nanoparticle on the flexural behaviors of the nanocomposites was determined from the three-point bending test in accordance with the ASTM

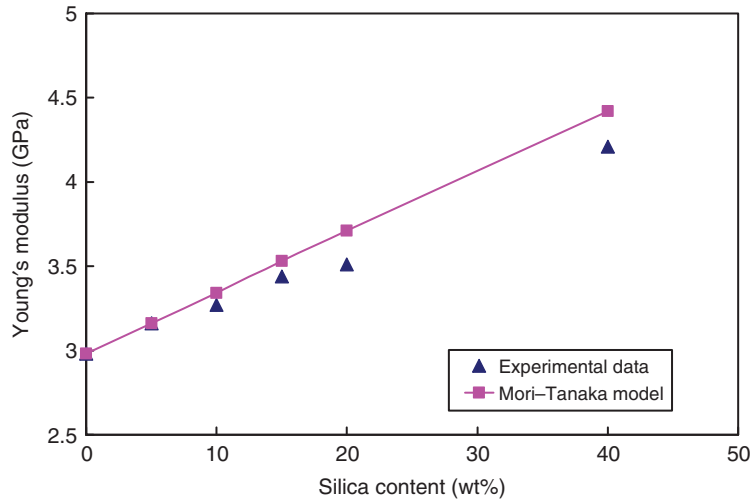

Figure 5. *Comparison of the experiments and model predictions for Young's modulus of nanocomposites with different silica loadings on ductile matrix.*

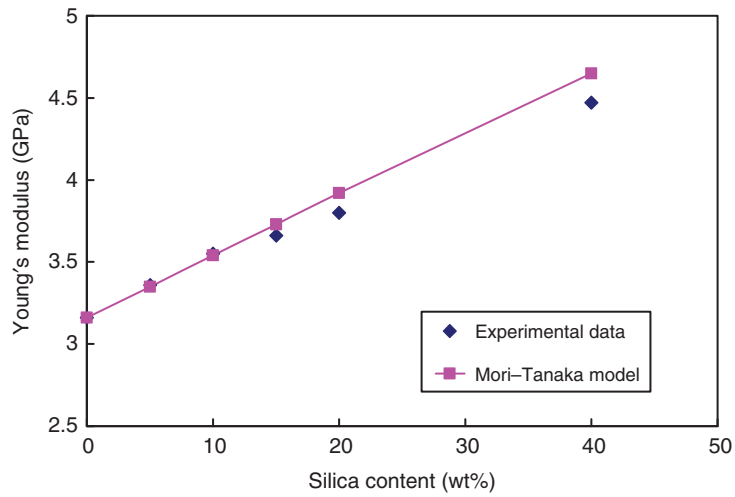

Figure 6. *Comparison of the experiments and model predictions for Young's modulus of nanocomposites with different silica loadings on brittle matrix.*

standard D790 [13]. During the tests, the crosshead is under stroke control, and the corresponding speed is set to be 1 mm/min. The flexural strength of the specimens is calculated from the following formulation:

$$S = \frac{3PL}{2bd^2} \tag{6}$$

where P is the applied failure load, L is the support span, and b and d represent the width and thickness of the specimens, respectively. Listed in Table 3 is the flexural strength of the nanocomposites with two different matrix systems. Results revealed that the flexural strength increases with the increment of particle loadings in both ductile and brittle cases.

Table 3. Effect of silica particle on flexural strength of nanocomposites with two different epoxy matrix systems.

Silica loading (wt%)	D-230 epoxy strength (MPa)	Increment ratio (%)	H-100 epoxy strength (MPa)	Increment ratio (%)
0	103.6	–	130.2	–
5	102.6	−1	131.7	1.2
10	106.4	2.7	134.8	3.5
15	106.1	2.4	141.4	8.6
20	112.2	8.3	146.8	12.7
40	120.5	16.3	155	19.0

The declining phenomena observed in the tensile strength for brittle matrix with 20 or 40 wt% loading of particle was not taking place in the flexural strength. Since the flexural strength is dominated by the local material property where the stress sates is high, it may not be as sensitive as the tensile strength to the specimen flaw.

MODE I FRACTURE TEST

In both tensile and flexural tests, results indicated that the nanocomposites with silica nanoparticles demonstrated higher stiffness and strength than the pure epoxy without any reinforcement. To further investigate the effect of the silica particle on the Mode I fracture toughness (K_{IC}), the single-edge-notch bending (SENB) specimens were fabricated and then employed for the three-point bending tests. The experiments were conducted basically following ASTM D5045 standards [14].

The dimensions of the SENB specimens are illustrated in Figure 7 where B denotes the thickness and W is the width of the sample. In an attempt to produce a sharp pre-crack tip, the pre-crack length (a in Figure 7) was created by a jewel saw followed by a new razor blade. The correlations of the dimensions $W = 2B$ and $a = B$, suggested by ASTM D5045, were followed during the preparations of SENB specimens with the thickness B around 6.2 mm. Moreover, in order to measure a valid fracture toughness, the following inequality equation for the specimen size must also be satisfied:

$$B, a, (W - a) > 2.5(K_I/\sigma_y)^2 \tag{7}$$

where σ_y is the yielding stress of the materials, determined using the offset method with 0.002 offset strains in the stress–strain curves shown in Figures 3 and 4. During the experiments, at least four specimens were tested in each case for the measurements of fracture toughness.

From the three-point bending tests, the fracture toughness of SENB samples can be calculated using the following formulation:

$$\begin{aligned} K_I &= \frac{P_I}{B\sqrt{W}} f(x) \\ f(x) &= 6x^{0.5} \frac{[1.99 - x(1-x)(2.15 - 3.93x + 2.7x^2)]}{(1+2x)(1-x)^{3/2}} \end{aligned} \tag{8}$$

where P_I indicates the peak load in the load and deflection curves, and x is a dimensionless value equal to the pre-crack length, a, divided by the sample width, W. The fracture tests were carried out on the servo-electrical control machine (HT-2102BP) at a displacement

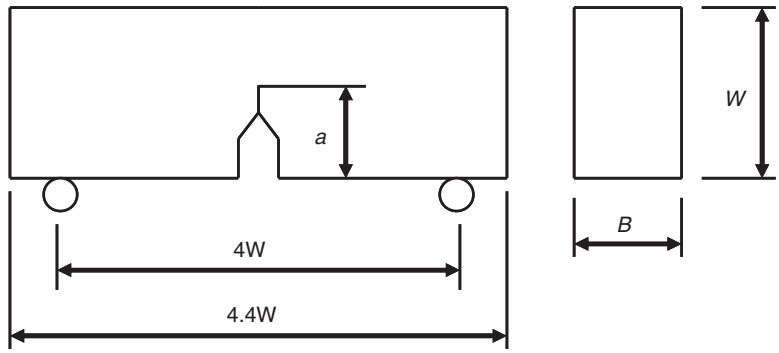

Figure 7. *SENB specimens for Mode I fracture tests.*

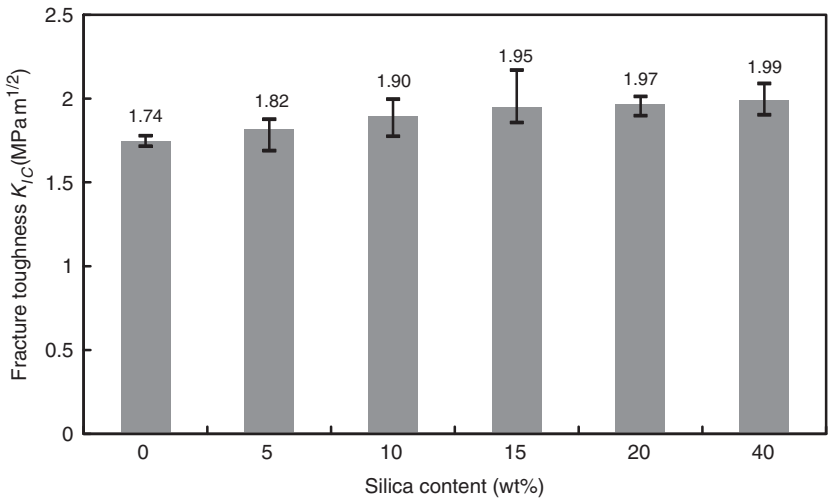

Figure 8. *Effect of silica particle loading on Mode I fracture toughness of nanocomposites with ductile epoxy systems.*

rate of 0.05 mm/min. The peak value of the force was regarded as the failure load, P_I, and employed in the calculation of the fracture toughness given by Equation (8). Figure 8 illustrates the variations of fracture toughness of the nanocomposites with ductile matrix containing different amounts of silica particles. Apparently, the fracture toughness of nanocomposites increases considerably with the addition of the silica particles, and the increasing tendency ceases as the particle loadings are greater than 10 wt%. The maximum enhancement was found to be 14% in the ductile epoxy system. On the other hand, for the nanocomposites with brittle matrix as shown in Figure 9, the fracture toughness consistently increases with the increment of the silica loadings up to 40 wt%, and the maximum improvement achieves around 80%. In contrast to tensile and flexural behaviors, the effect of silica particles on the fracture toughness relies on the matrix system.

In order to investigate the mechanism resulting in the enhancement of fracture toughness, the failure surfaces of the specimens around the crack tips were examined using SEM with low and high magnifications. From the low magnification micrograph as shown in Figure 10, it is depicted that the significant river-type marks near the crack tip were found,

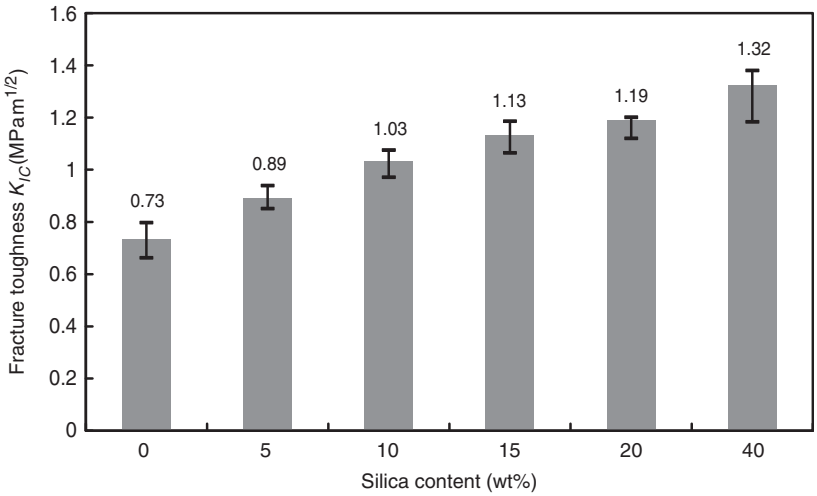

Figure 9. *Effect of silica particle loading on Mode I fracture toughness of nanocomposites with brittle epoxy systems.*

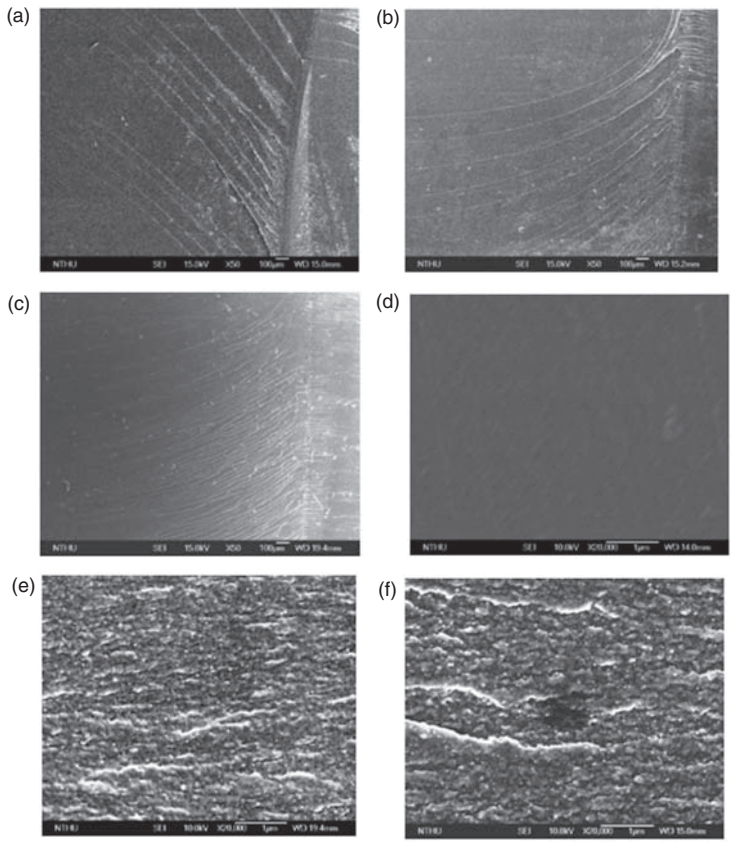

Figure 10. *SEM micrograph for ductile matrix nanocomposites with 0, 10, and 40 wt% of silica particles: (a) 0 wt%, 50 magnification, (b) 10 wt%, 50 magnification, (c) 40 wt%, 50 magnification, (d) 0 wt%, 20 K magnification, (e) 10 wt%, 20 K magnification, (f) 40 wt%, 20 K magnification).*

indicating the typical fractography of ductile failure behavior. The density of the river-type marks is higher in the nanocomposites with 10 and 40 wt% of silica particles as compared to the pure epoxy sample. The fracture surfaces of the nanocomposites were further examined using SEM with high magnification. It is interesting to note that for the pure epoxy, the surface is practically smooth and featherless. In contract, for the nanocomposites, the surface is rough with some miniature cavitations that may be caused by the localized plastic deformation of the matrix accompanied with the interfacial debonding between the particle and surrounding matrix. This failure mechanism may complicate the fracture process and dissipate more fracture energy for crack initiation, resulting in high fracture toughness. The extent of the surface roughness for the nanocomposites with 10 and 40 wt% particles were quantitatively measured using AFM as shown in Figure 11. Apparently, the surface roughness for the two cases are almost the same, which is the

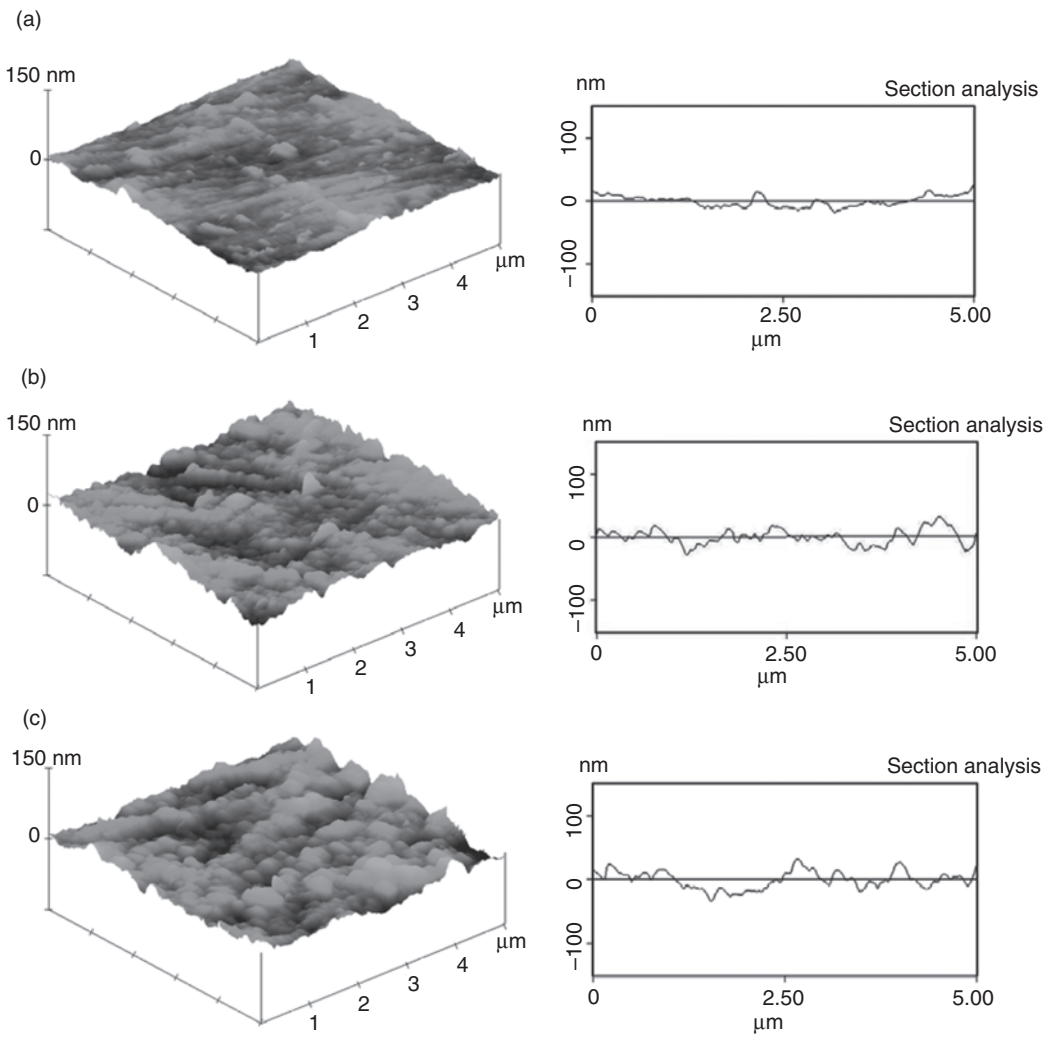

Figure 11. *Fracture surface profile of ductile matrix nanocomposites with with 0, 10, and 40 wt% of silica particles measured from AFM: (a) 0 wt%, (b) 10 wt%, (c) 40 wt%.*

reason why the fracture toughness for the nanocomposites with particle loading ranges from 10 to 40 wt% are not altered.

For the nanocomposites with the brittle matrix, the fracture surfaces observed using SEM and AFM were shown in Figures 12 and 13, respectively. It can be seen that for the pure epoxy resin, no clear river pattern is observed on the low magnification SEM micrographs. On the other hand, the river pattern begins to appear on the fracture surfaces of nanocomposites, and the density of the pattern increases with the increment of silica loadings. Moreover, from the high magnification SEM micrographs, it is revealed that the fracture surface is pretty rough at the samples with higher silica particle loading. The rough fracture surface may be responsible for the increased fracture toughness of the nanocomposites. Again, the surface profiles of the nanocomposites were measured using AFM as shown in Figure 13. It is shown that for the composites with 40 wt% silica particles, the surface roughness is significant, coinciding with our SEM observations.

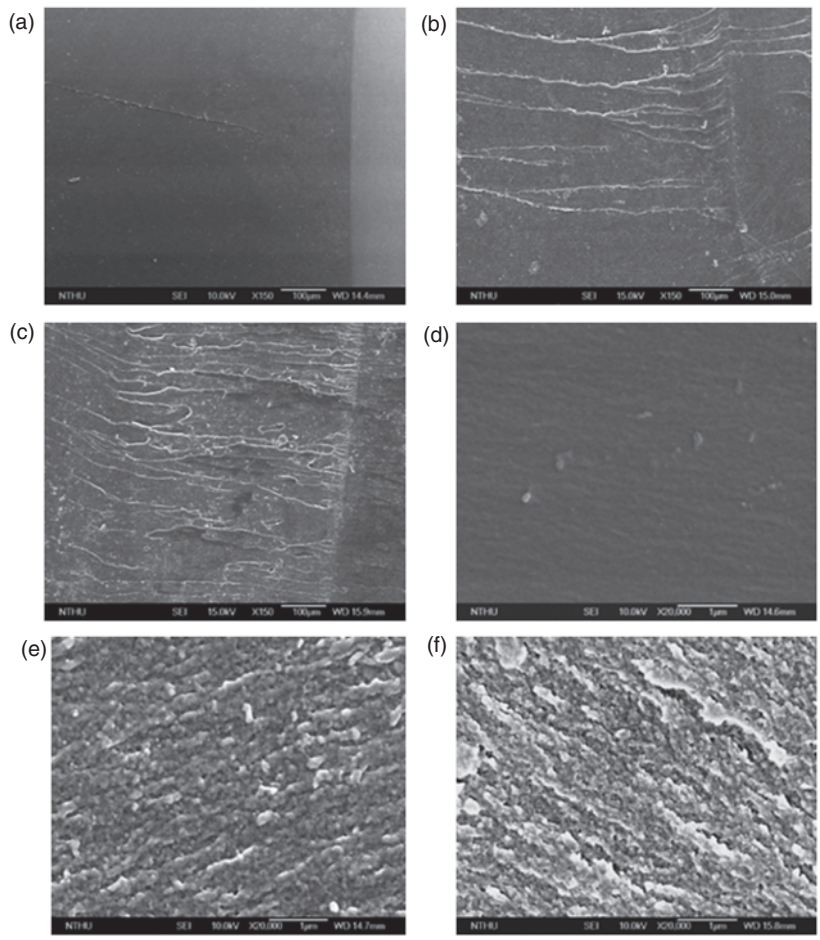

Figure 12. *SEM micrograph for brittle matrix nanocomposites with 0, 10, and 40 wt% of silica particles: (a) 0 wt%, 150 magnification, (b) 10 wt%, 150 magnification, (c) 40 wt%, 150 magnification, (d) 0 wt%, 20 K magnification, (e) 10 wt%, 20 K magnification, (f) 40 wt%, 20 K magnification.*

Glass Fiber/Silica/Epoxy Nanocomposites

In view of the forgoing that the mechanical properties of the nanocomposites, such as stiffness, strength, and fracture toughness, can be improved dramatically by the inclusion of the silica nanoparticles, but for the purpose of structural applications, the improvement made by nanoparticles may not be significant enough when compared to that by using the long fibers in the conventional composites. If we can comprise the advantage of the silica nanoparticles with the conventional fiber composites to form the fiber-reinforced hybrid nanocomposites, the mechanical properties of the hybrid system may be superior to the conventional one. To achieve this goal, the unidirectional fiber hybrid nanocomposites were prepared, and the effect of the nanoparticle on the corresponding mechanical properties was evaluated. In this study, the mechanical behaviors of fiber composites dominated

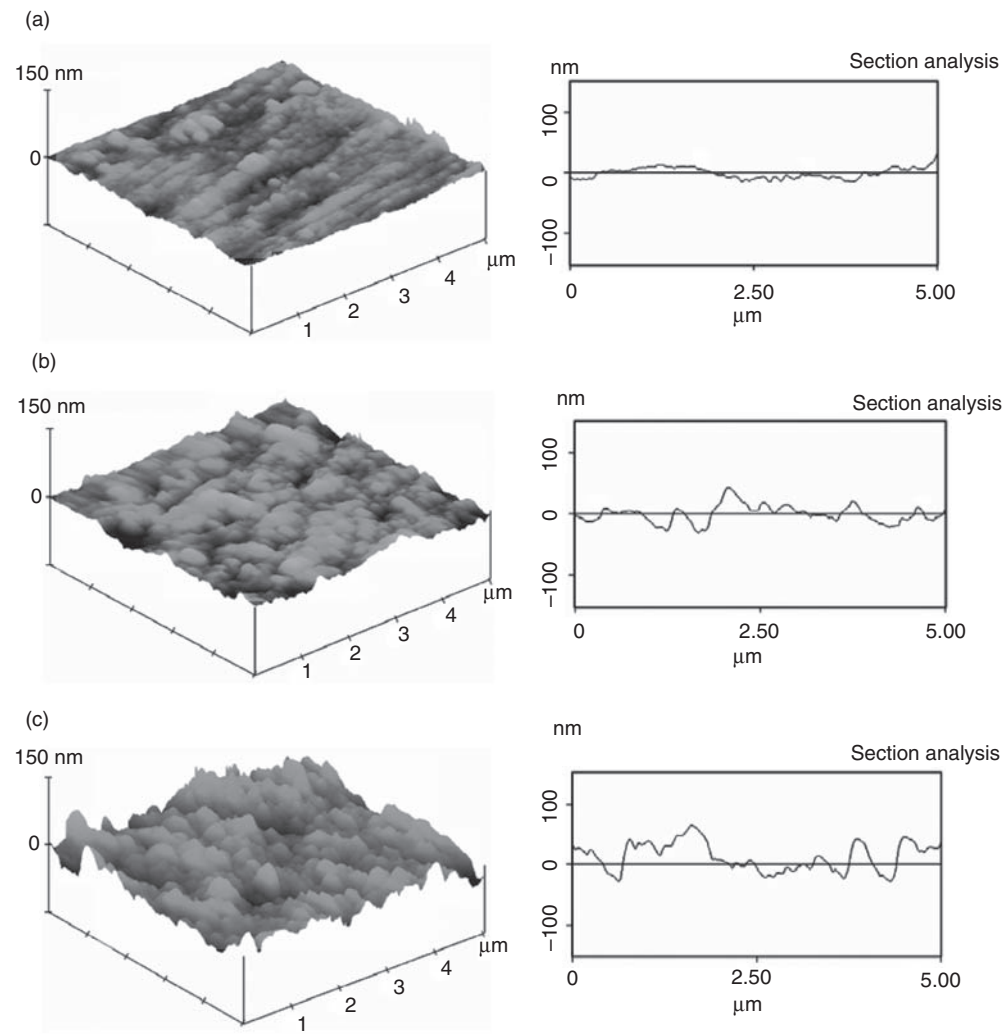

Figure 13. *Fracture surface profile of brittle matrix nanocomposites with 0, 10, and 40 wt% of silica particles measured from AFM: (a) 0 wt%, (b) 10 wt%, (c) 40 wt%.*

by the matrix properties, such as in-plane shear strength and off-axis compressive strength, were of concern.

IN-PLANE SHEAR STRENGTH

The in-plane shear property was characterized by conducting tensile tests on the 10° off-axis specimens. The dimension of 10° off-axis specimens is illustrated in Figure 14. It is noted that the oblique end taps were used on the specimens to diminish the extension and shear coupling effect caused by off-axis loading [15].

The in-plane shear strength obtained from the off-axis 10° specimens are listed in Table 4, which are associated with different silica nanoparticle loadings. It is revealed that in-plane shear strength increases as the silica particle loading rises and accomplishes the peak value at 10 wt% loading of silica nanoparticles. The SEM micrographs on the facture surfaces of the samples are shown in Figure 15. It was indicated that for the conventional fiber composites, the fiber surfaces are quite smooth without any matrix attached, which is apparently the symptom of an interfacial debonding failure mechanism. Nevertheless, for the nanocomposites with silica nanoparticles, the fiber surfaces are attached with the epoxy together with some particle aggregations. The agglomerations may increase the interfacial bonding between the fiber and matrix such that when the fracture initiates, the matrix failure and interfacial debonding may occur simultaneously. Thus, by modifying the interfacial property of fiber and surrounding matrix, the silica nanoparticles can enhance the in-plane shear strength of the nanocomposites noticeably. In addition, it was noted that when 20 wt% silica nanoparticles were loaded, the samples

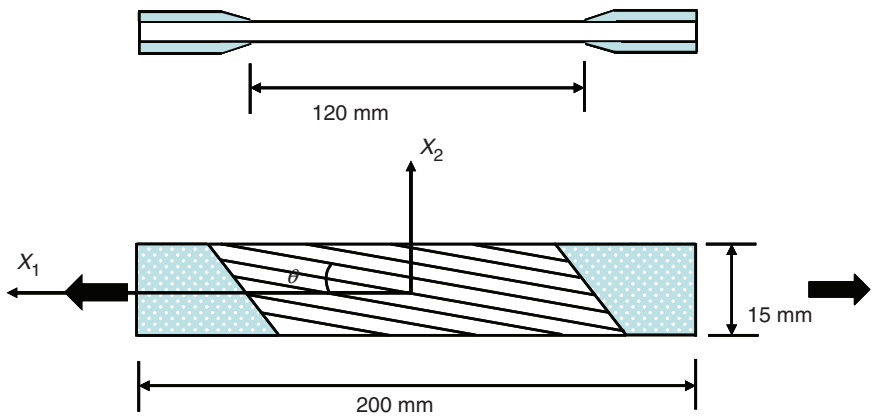

Figure 14. *Dimension of 10° off-axis specimen for tensile test.*

Table 4. Effect of silica particle on in-plane shear strength of nanocomposites.

Silica loading (wt%)	In-plane shear strength (MPa)	Increment ratio (%)
0	23.7	–
5	27.5	16.0
10	30.1	27.0
20	29.6	24.9

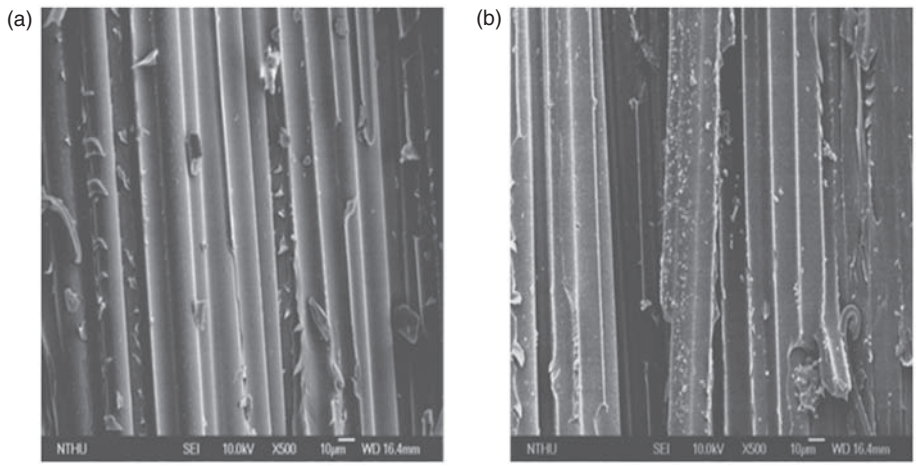

Figure 15. *SEM micrograph on the fracture surfaces of the samples: (a) pure epoxy matrix, (b) epoxy matrix containing 20 wt% silica particles.*

exhibited a little lower in-plane shear strength than the 10 wt% silica nanocomposites. This decreasing behavior could be due to the high viscosity of the 20 wt% silica epoxy matrix which makes it difficult to completely wet the fibers during the hand lay-up process. Therefore, the flaws could be generated in the samples and result in the reduction of in-plane shear strength.

OFF-AXIS COMPRESSIVE STRENGTH

In order to verify the silica particle influence on the compressive strength of fiber composites, compressive failure tests were conducted on glass epoxy composite specimens with 20 wt% silica particles. The results were compared to those obtained from the specimens without any silica nanoparticles included. Off-axis brick specimens (dimensions as shown in Figure 16) with fiber orientations of 0°, 5°, 10°, 15°, and 90° (against the long direction), respectively, were cut from a 22-ply unidirectional glass epoxy laminate using a diamond wheel. The specimens were lapped on a lapping machine with a 6 μm abrasive slurry to ensure smooth and flat loading surfaces and then tested in compression by means of the end loading condition with a pair of tungsten carbide disks as shown in Figure 17. In addition, a lubricant was applied to the end surfaces of the specimen to reduce contact friction. A self-adjusting device, as shown in Figure 17, was used to eliminate potential bending moments and also to ensure that the specimen was in full contact with the loading surfaces. All tests were conducted at hydraulic MTS machine with strain rate of 0.0001/s. The applied load and displacement for each test were recorded using Lab VIEW software with a PC computer.

All failed specimens from the tests were examined using a microscope to observe the failure mechanisms. For the 5°, 10°, and 15° specimens, fiber microbuckling was found to be the dominant failure mechanism. For the 0° specimens, the failure mechanism was mainly dominated by fiber splitting. Figure 18 shows the failure mechanism of fiber microbuckling in the 5° and 10° off-axis glass/silica/epoxy/composite specimens. On the other hand, for 90° samples, the out-of-plane shear failure mechanism was observed to the main failure mechanism as shown in Figure 19. Moreover, from the experimental observations, it was found that the failure mechanisms were basically not

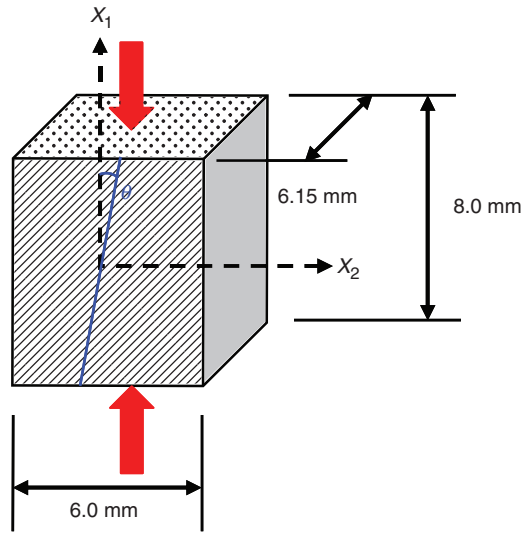

Figure 16. *Dimension of brick specimen for compression tests.*

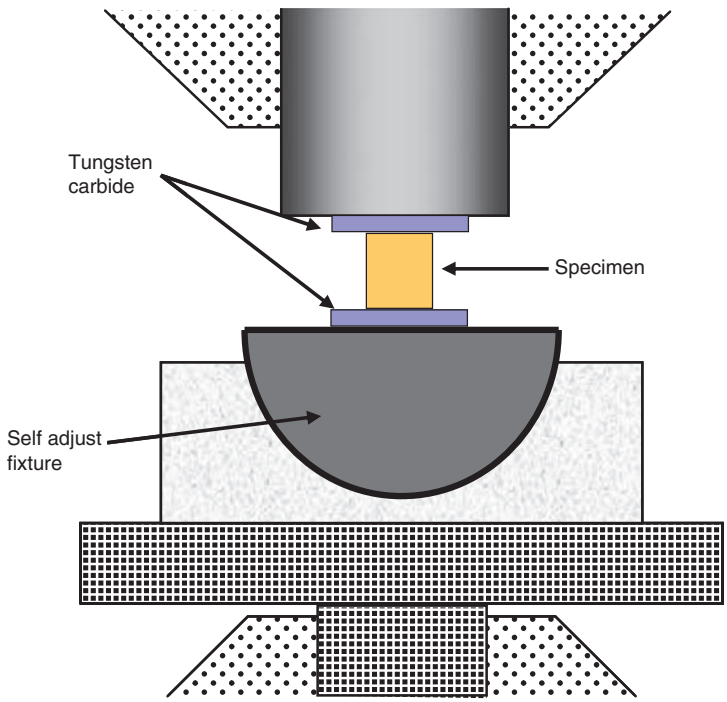

Figure 17. *Schematic of compression tests.*

altered by the silica nanoparticles. Nevertheless, the failure stresses of the off-axis samples were enhanced appreciably by the silica nanoparticles as shown in Table 5.

The enhanced behavior of the compressive strength for the 5°, 10°, and 15° specimens can be described using the microbuckling model [16]. Rosen employed a 2D elastic model

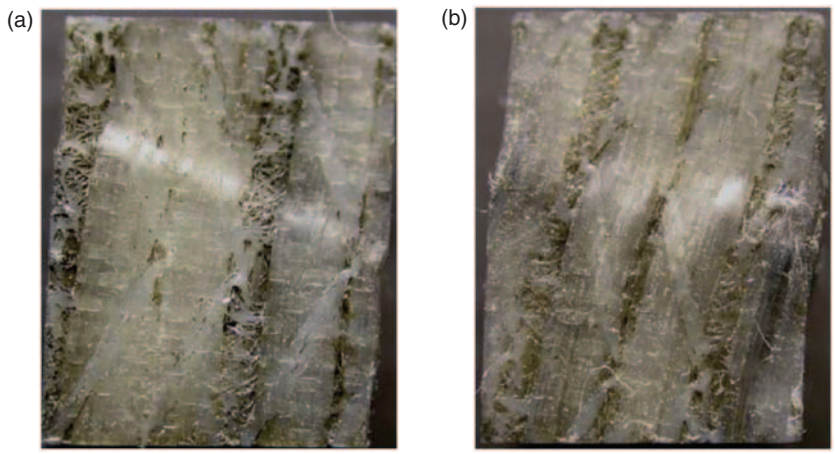

Figure 18. *Microbuckling failure mechanism in 5° and 10° off-axis glass fiber/silica/epoxy specimens: (a) 5°, (b) 10°.*

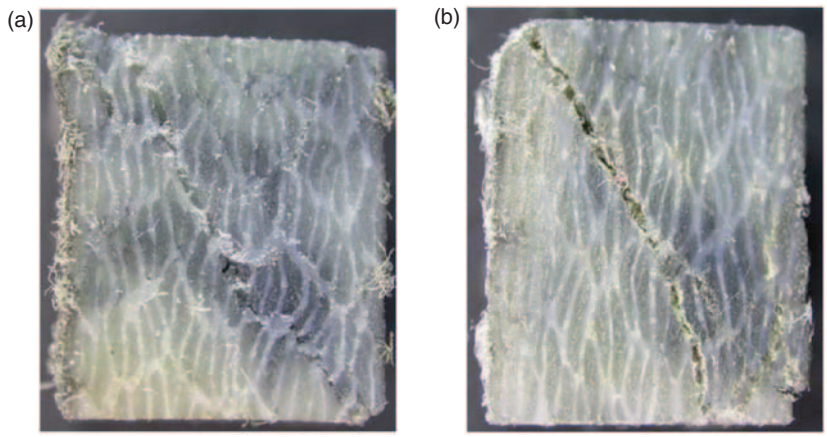

Figure 19. *Out-of-plane shear failure mechanism in 90° specimens: (a) glass/epoxy specimen, (b) glass/silica/epoxy specimen.*

Table 5. Comparison of compressive strengths of off-axis composite samples with/without silica particles.

Fiber orientation	Compressive strength (MPa)	Compressive strength (MPa) (with silica 20 wt%)	Increment (%)
0	414.8	445.3	7.4
5	226.8	265.1	16.9
10	154.1	163.3	6
15	117.2	123.6	5.5
90	46	47	2.2

to estimate the microbuckling condition of fibers in a composite, indicating that the buckling stress of the dominant shear mode is given by [17]:

$$\sigma_{11c} = \frac{G_m}{1 - c_f} \tag{9}$$

where G_m is the shear modulus of the matrix, and c_f denotes the fiber volume fraction of the composites. According to Equation (9), it is suggested that the compressive strength of the composites can be significantly enhanced if the shear modulus of the matrix is improved. From the previous investigation, it was suggested that the Young's modulus of the epoxy matrix can be modified by the nanoparticles. If we assumed the epoxy matrix as an isotropic material with constant Poisson's ratio, the corresponding shear modulus can be increased properly by the nanoparticles. Therefore, it is not surprised that 5°, 10°, and 15° specimens with 20 wt% silica particles demonstrate superior compressive strengths than those with pure epoxy matrix. It is noted that in Equation (9), the microbuckling stress is evaluated in the fiber direction, and the sensitivity of the failure stress for the off-axis specimens in the form of fiber microbuckling is dependent on the fiber orientation to the loading direction. Moreover, for the 0° and 90° samples, although the failure mechanisms are different from the fiber microbuckling, the composites with 20 wt% silica nanoparticles still exhibit higher failure stresses than those that do not contain any silica particles.

CONCLUSIONS

The tensile, flexural, and fracture behaviors of nanocomposites with two different matrix systems containing different silica nanoparticle loadings were investigated experimentally in this study. From the tensile tests, it was found that the tensile strength and stiffness increase with the increment of nanoparticle loadings, and the increasing behaviors can be described properly using the Mori–Tanaka micromechanical model. With regard to the fracture behavior, for the ductile matrix system, the increment ratio is around 15% at 40 wt% of nanoparticle content. On the other hand, for the brittle system with 40 wt% nanoparticles, the enhancement can achieve to 80%. From SEM and AFM observations on the failure surfaces, it was indicated that the increment of fracture toughness was due to the plastic deformation accompanied with the nanoparticle debonding, which may consume more fracture energy and complicate the fracture extension.

For the glass fiber composite specimens, the in-plane shear strength was improved by the addition of silica nanoparticle into epoxy matrix. The ascending phenomena could be attributed to the improved interfacial bonding between fibers and surrounding epoxy caused by the presence of the silica nanoparticles. Moreover, from the compression tests on 0°, 5°, 10°, 15°, and 90° off-axis samples, it was found that the fiber composites with 20 wt% silica particles exhibit higher failure stresses than those with pure epoxy matrix. For 5°, 10°, and 15° samples, the main failure mode is the fiber microbuckling, the failure stress of which can be enhanced appropriately by the improvement of the shear modulus of the matrix material made by silica nanoparticles.

REFERENCES

1. Han, J.T. and Cho, K. (2006). Nanoparticle-induced Enhancement in Fracture Toughness of Highly Loaded Epoxy Composites Over a Wide Temperature Range, *Journal of Materials Science*, **41**(13): 4239–4245.
2. Wu, C.L., Zhang, M.Q., Rong, M.Z. and Friedrich, K. (2002). Tensile Performance Improvement of Low Nanoparticles Filled-polypropylene Composites, *Composites Science and Technology*, **62**(10): 1327–1340.
3. Bugnicourt, E., Galy, J., Gerad, J.F. and Barthel, H. (2007). Effect of Sub-micron Silica Fillers on the Mechanical Performances of Epoxy-based Composites, *Polymer*, **48**(6): 1596–1605.
4. Cho, J., Joshi, M.S. and Sun, C.T. (2006). Effect of Inclusion Size on Mechanical Properties of Polymeric Composites with Micro and Nano Particle, *Composites Science and Technology*, **66**(13): 1941–1952.
5. Chin, I., Thurn-Albrecht, T., Kim, H., Russell, T.P. and Wang, J. (2001). On Exfoliation of Montmorillonite in Epoxy, *Polymer*, **42**(13): 5947–5952.
6. Adebahr, T., Roscher, C. and Adam, J. (2001). Reinforcing Nanoparticles in Reactive Resins, *European Coatings Journal*, **4**: 144–149.
7. Rosso, P., Ye, L., Friedrich, K. and Sprenger, S. (2006). A Toughened Epoxy Resin by Silica Nanoparticle Reinforcement, *Journal of Applied Polymer Science*, **100**(3): 1849–1855.
8. Johnsen, B.B., Kinloch, A.J., Mohammed, R.D., Taylor, A.C. and Sprenger, S. (2007). Toughening Mechanisms of Nanoparticle-modified Epoxy Polymers, *Polymer*, **48**(2): 530–541.
9. Deng, S., Ye, L. and Friedrich, K. (2006). Fracture Behaviours of Epoxy Nanocomposites with Nano-silica at Low and Elevated Temperatures, *Journal of Materials Science*, **42**(8): 2766–2774.
10. Zheng, Y. and Ning, R. (2005). Study of SiO_2 Nanoparticles on the Improved Performance of Epoxy and Fiber Composites, *Journal of Reinforced Plastics and Composites*, **24**(3): 223–233.
11. Mori, T. and Tanaka, K. (1973). Average Stress in Matrix and Average Elastic Energy of Materials with Misfitting Inclusions, *Acta Metallurgica*, **21**(5): 571–574.
12. Mura, T. (1982). *Micromechanics of Defects in Solids*, Martinus Nijhoff, The Hague.
13. ASTM D790-97 (1997). Standard Test Methods for Flexural Properties of Plastics and Electrical Insulating Material, Annual Book of ASTM Standard.
14. ASTM D5045-97 (1997). Standard Test Methods for Plane-strain Fracture Toughness and Strain Energy Release Rate of Plastic Materials, Annual Book of ASTM Standard.
15. Sun, C.T. and Chung, I. (1993). An Oblique End-tab Design for Testing Off-axis Composite Specimens, *Composites*, **24**(8): 619–623.
16. Tsai, J. and Sun, C.T. (2004). Dynamic Compressive Strengths of Polymeric Composites, *International Journal of Solids and Structures*, **41**(11–12): 3211–3224.
17. Rosen, B.W. (1965). *Mechanics of Composite Strengthening in Fiber Composites Materials*, pp. 35–75, American Society of Metals, Metals Park, OH.